IEEE Access
Multidisciplinary ⋮ Rapid Review ⋮ Open Access Journal

Received 8 October 2022, accepted 19 October 2022, date of publication 26 October 2022, date of current version 7 November 2022.

Digital Object Identifier 10.1109/ACCESS.2022.3217237

RESEARCH ARTICLE

Back-Stepping Formation Control of Unmanned Surface Vehicles With Input Saturation Based on Adaptive Super-Twisting Algorithm

ZOU YUHAN[1], WANG KUN[2], SHANG WEI[1], LIU ZHOU[1], ZHENG ZHONGZHONG[1], AND JING GUO HAO[1]

[1]School of Mechanical Engineering, Hubei University of Technology, Wuhan 430068, China
[2]China Ship Development and Design Center, Wuhan 430064, China

Corresponding author: Wei Shang (bitshw@126.com)

This work was supported by the Collaborative Innovation Center of Intelligent Green Manufacturing Technology and Equipment, Shandong, under Grant IGSD-2020-007.

ABSTRACT Aiming at the formation control problem for unmanned surface vehicles under input overload and external disturbance, a leader-follower formation control law based on input saturation and the adaptive super-twisting algorithm was designed in this paper. Firstly, the mathematical model of underactuated unmanned surface vehicle formation based on the leader-follower method is established, and the virtual expected velocity is designed by the back-stepping method to improve the control accuracy of formation. Secondly, the parametric uncertainties and unknown external disturbances in the USV's dynamical model are compensated by the proposed adaptive super-twisting control laws. In addition, the input saturation function is added to the controller to avoid machine necrosis caused by input overload. Finally, Simulation results show that the controller can roughly keep the trajectory of the USV consistent with the expected trajectory and ensure that the input values are within the safe range, which proves the effectiveness of the method in this paper.

INDEX TERMS Unmanned surface vehicles, multi-agent system, super-twisting algorithm, input saturation.

I. INTRODUCTION

With the rapid development of unmanned intelligent systems and the growing demand for unmanned surface vehicles(USVs), USVs formation is gradually coming to researchers' minds. Due to the limitations of a single USV operation, a single USV can not efficiently complete or even complete complex tasks, with a small operating range and poor fault tolerance. Scholars are currently conducting extensive research on the performance of USV formations in some special missions [1], [2], [3], [4], [5]. Multiple USVs operating at the same time can enable marine operations to be more durable, intelligent and large-scale, becoming one of the important development trends of future marine operations. Meanwhile, due to the diversity of tasks and the complexity of the external environment [6], the control performance of the USV formation is increasingly required, which greatly affects the stability of the USV formation.

USVs can be mainly divided into underactuated USVs and fully actuated USVs. The fully actuated USVs haye a lateral swing direction control mechanism, which can provide the lateral swing direction of power. However, considering that most USVs are only equipped with propellers and rudders in the transverse swing direction in practical applications, this under-actuated system cannot be transformed into a drift-free system. In [7], and [8], neural networks (NNs) are used to approximate the uncertainty of the USV model and realize the ideal formation mode. However, the problems of external interference and input overload are not considered. In order to solve the problem of underactuated USV formation control in a complex external environment, a leader-follower formation control law based on saturation safety constraints and the adaptive super-twisting algorithm was designed in this paper, which is more suitable for the actual application and more in line with the genuine demand of underactuated USV.

The associate editor coordinating the review of this manuscript and approving it for publication was Jinquan Xu.

There have been many research achievements in improving the accuracy of formation control and maintaining the formation state [1], [9], [10]. In [9], a Bio-Inspired Method based on a virtual leadership strategy is proposed to ensure the organization's stability and reduce disturbance through coordination transformation. By combining virtual structure with the artificial potential field, the USV can maintain high formation accuracy and formation change flexibility [10]. The formation control model based on deep reinforcement learning (DRL) was constructed in [1] to promote USV to form preset formation. However, to solve the problem that the upper and lower bounds of the external disturbance of USVs formation are unknown, this paper introduces the adaptive super-twisting algorithm on the conventional formation control strategy to compensate for the external disturbance so that the accuracy of formation control is better guaranteed.

Back-stepping control is a recursive design method with high robustness when disturbance and uncertainty do not meet the matching conditions, and has been widely studied in formation control [11], [12], [13], [14], [15]. In order to improve the robustness of the control system under model uncertainty and environmental interference, Sun Z al. proposed a robust adaptive trajectory tracking algorithm based on proportional integral sliding mode control and back-stepping technology [11]. In [12], a sliding mode controller based on approach law and adaptive back-stepping execution are designed to improve the disturbance rejection accuracy of USV. In [13], an adaptive technique based on back-stepping sliding mode theory is introduced to compensate for model uncertainties and time-varying disturbances of the system, which enhances the robustness of the underactuated USV in unknown environments. In [14], a control method combining adaptive back-stepping technique and sliding mode is proposed to achieve a smooth transition of formations and cope with various uncertain disturbances. In [15], a Lyapunov-based back-stepping controller is proposed to successfully achieve cooperative motion control of multiple underwater robots in discrete data transmission. Inspired by the above literature, this paper uses back-stepping control in the controller's design to improve the formation control's stability.

During work time, USVs are inevitably subject to external environmental influences that interfere with the normal operating conditions of the USVs. Therefore, how to realize convergence of USV in finite time has been widely studied, and finite time convergence control can achieve faster convergence speed and provide higher control precision and anti-interference ability. Among them, the adaptive super-twisting (AST) scheme is a second-order continuous sliding mode control algorithm with relative degrees equal to 1. When the bound is known and smooth matching perturbations with bounded gradients is existent, a continuous control function is generated and the sliding variable and its derivative are driven to zero in a finite time. It has been widely studied in academia because of its fast convergence speed and high convergence accuracy. [14], [15], [16], [17], [18], [19]. In order to improve the tracking performance, Qiu B designs an im- proved fast and super fast nonlinear sliding mode controller for nonlinear sliding surfaces [14]. In [18], to ensure the ideal performance of uncertain nonlinear systems, a new adaptive super-twisting structure is designed to solve the problem of uncertain matching and mismatching nonlinear systems. However, the literature above does not guarantee finite time convergence in the upper and lower bounds of unknown systems and perturbations. Adopting the adaptive algorithm enables us to eliminate the boundary information of the lumping uncertainties. The tracking controller in this paper adopts super-twisting control to ensure the formation convergence of USV in finite time under unknown initial conditions.

When the USV is working on the water surface, the control force and control torque required by the USV may exceed the maximum control force and control torque it can provide when resisting external interference and achieving tracking targets, so that the dynamic performance of the USV formation will become low, the closed-loop system may become unstable, and it is easy to lead to collisions between USVs. Saturation control is a safety constraint for setting upper and lower limits on the control rate at the control terminal so that it is within the limits that the system can withstand. Qiu B introduced smoothing assistant system in tracking path to alleviate the influence of input saturation [20]. In [21], neural network minimum learning parameter method and disturbance observer are used to compensate the unmodeled dynamic disturbance and external disturbance respectively. In [22], RBF network was used to approximate the input saturation of the system, and optimization was carried out through genetic algorithm. The safety constraint used in this paper is a constraint function attached to the adaptive super-twisting controller, which is used to further improve the dynamic stability of the USV formation and avoid input overload problems.

Motivated by the above discussion, we note some research results on sliding mode control of USVs and the application of saturation control in the presence of input saturation, which are instructive for our research work. Unlike the controller designed in [23] that cannot achieve finite-time convergence and guarantee the USV's dynamic performance in input saturation when the upper and lower limits of disturbance are unknown. Compared with existing USVs formation methods, we have the following four advantages: 1. Faster convergence, higher control precision and stronger robustness. Benefiting from the adaptive super-twisting (STW) scheme, the USVs can maintain tracking stability and good control accuracy despite disturbances from external factors. 2. The boundary information is no longer needed, thanks to the adaptive algorithm that eliminates the lumping uncertainty. 3. Better formation retention capability. The leader-follower control and back-stepping method are used to improve the stability of formation control. 4. Avoid the input overload problem. The use of saturation control provides greater stability in USV formations.

The contributions in this paper are as follows. 1. To achieve trajectory tracking under uncertainty, a controller based

on leader-follower control and back-stepping method is designed to improve the stability of formation control. 2. The controller uses adaptive super-twisting control, which enables the USV to maintain tracking stability and good control accuracy despite disturbances from external factors. 3. To avoid the input overload problem, the controller uses input saturation control to make the dynamic performance of the USV formation more stable.

II. PROBLEM DESCRIPTION

The motion of USV is a compound motion in three-dimensional space, which is composed of linear motion and rotational motion around three coordinate axes. The motions of the six free degrees are as follows: 1) longitudinal oscillation along x-axis and transverse oscillation around x-axis; 2) transverse oscillation along y-axis and longitudinal oscillation around y-axis; 3) vertical oscillation along z-axis and bow oscillation around z-axis. Since the effects of vertical, longitudinal and transverse oscillation can be ignored for navigation on river water in this paper, the model can be simplified to a nonlinear model with three degrees of freedom. The mathematical model is described as follow:

Define water surface coordinate system O_eX_eY. $o_bx_by_b$ is the system coordinate system. The formation system consists of many USVs, define the model of the i_{th} USV:

$$\begin{cases} \dot{x}_i = u_i \cos(\varphi_i) - v_i \sin(\varphi_i) \\ \dot{y}_i = u_i \sin(\varphi_i) + v_i \cos(\varphi_i) \\ \dot{\varphi}_i = r_i \\ M_i \dot{V}_i + C_i(v_i) V_i + D_i(v_i) V_i + \Delta d = \tau_i \end{cases} \tag{1}$$

where (x_i, y_i) is the coordinates of the i_{th} USV under O_eX_eY. The heading of the i_{th} USV is respectively defined as φ_i, u_i, v_i and r_i are the longitudinal velocity, the transverse velocity and the bow-roll velocity of the i_{th} USV respectively, $V_i = [u_i, v_i, r_i]^T$, $i = 1, 2 \ldots n$; $\tau_i = \begin{bmatrix} \tau_{iu} & 0 & \tau_{ir} \end{bmatrix}^T$ is the control input of USV; $M_i = \begin{bmatrix} m_{11} & 0 & 0 \\ 0 & m_{22} & 0 \\ 0 & 0 & m_{33} \end{bmatrix}$ is the Coriolis force and centripetal acceleration matrix of the USV; $D_i(v_i) = \begin{bmatrix} d_{11} & 0 & 0 \\ 0 & d_{22} & 0 \\ 0 & 0 & d_{33} \end{bmatrix}$ is the damping matrix of the USV. $\Delta d = \begin{bmatrix} \Delta d_u & 0 & \Delta d_r \end{bmatrix}^T$ is the unknown external disturbance.

A. FORMATION MODEL OF USVs

The leader-follower method is used to control the formation of USVs in this paper. As shown in Figure 1, one USV in the formation is designated as the leader. In practice, we use the latitude and longitude information obtained by GPS to determine the position information between USVs. L is the distance between the two USVs, L_x and L_y are the transverse and longitudinal distances of the two ships. By making the actual distance L between the leader and follower close to the expected distance L_d, we can realize the formation control of multiple USVs.

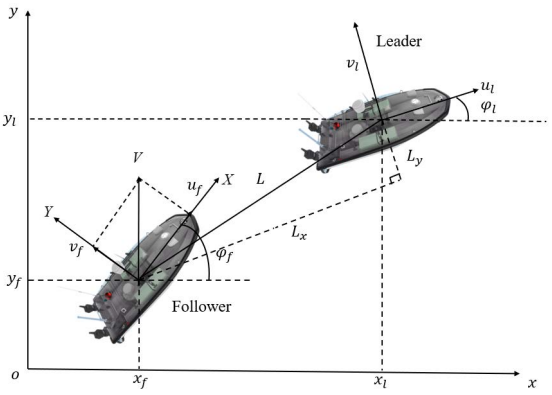

FIGURE 1. Leader-follower model.

From Figure 1, it can be seen that the relative position relationship between the leader and the follower is

$$\begin{cases} L_x = -(x_{il} - x_{if}) \cos\varphi_{il} - (y_{il} - y_{if}) \sin\varphi_{il} \\ L_y = (x_{il} - x_{if}) \sin\varphi_{il} - (y_{il} - y_{if}) \cos\varphi_{il} \end{cases} \tag{2}$$

Take the derivative of both sides and we get the following:

$$\begin{cases} \dot{L}_x = -u_{il} + u_{if} \cos e_\varphi + v_{if} \sin e_\varphi + L_y r_{il} \\ \dot{L}_y = -v_{il} - u_{if} \sin e_\varphi + v_{if} \cos e_\varphi - L_x r_{il} \end{cases}$$

Among the formulas, θ_d represents the expected relative angle of the leader and the follower, and L_d represents the expected relative distance between them. Then, the error in the x and y directions is

$$\begin{cases} e_x = L_x - L_d \cos\theta_d \\ e_y = L_y - L_d \sin\theta_d \end{cases} \tag{3}$$

Take the derivative of both sides of (3) and we get the model of the USV formation

$$\begin{cases} \dot{e}_x = u_{if} \cos e_\varphi + v_{if} \sin e_\varphi + e_y r_{il} + f_1 \\ \dot{e}_y = -u_{if} \sin e_\varphi + v_{if} \cos e_\varphi - e_x r_{il} + f_2 \\ \dot{e}_\varphi = r_{il} - r_{if} \\ \dot{u}_{if} = \frac{m_{2f}}{m_{1f}} v_{if} r_{if} - \frac{d_{1f}}{m_{1f}} u_{if} + \frac{1}{m_{1f}} \tau_{iuf} + \Delta d_u \\ \dot{v}_{if} = -\frac{m_{1f}}{m_{2f}} u_{if} r_{if} - \frac{d_{2f}}{m_{2f}} v_{if} \\ \dot{r}_{if} = \frac{m_{1f} - m_{2f}}{m_{3f}} u_{if} v_{if} - \frac{d_{3f}}{m_{3f}} r_{if} + \frac{1}{m_{3f}} \tau_{irf} + \Delta d_r \end{cases} \tag{4}$$

where τ_{iuf} and τ_{irf} are the forward thrust and bow rolling moment of the follower respectively; f_1 and f_2 are defined as follows:

$$\begin{cases} f_1 = -u_{il} - \dot{L}_{d_y} + L_{d_y} r_{il} \\ f_2 = -v_{il} - \dot{L}_{d_x} - L_{d_x} r_{il} \end{cases} \tag{5}$$

To illustrate the idea and design of the leader-follower approach in this paper more accurately, we have added more descriptions and added a navigator-follower topology diagram as shown in figure 2.

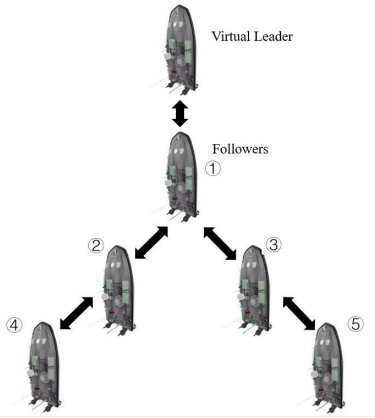

FIGURE 2. Leader-follower topology diagram.

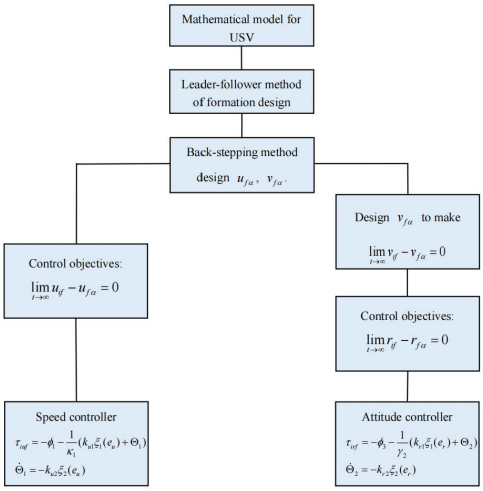

FIGURE 3. Formation control block diagram.

B. FORMATION CONTROL GOAL

(a) In order to make $L_x \to L_{d_x}$, $L_y \to L_{d_y}$, we design the virtual lateral velocity $u_{f\alpha}$ and virtual longitudinal velocity $v_{f\alpha}$ of the following ship such that

$$\begin{cases} \lim\limits_{t\to\infty} \left\| L_x - L_{d_x} \right\| = \lim\limits_{t\to\infty} \left\| e_x \right\| = 0 \\ \lim\limits_{t\to\infty} \left\| L_y - L_{d_y} \right\| = \lim\limits_{t\to\infty} \left\| e_y \right\| = 0 \end{cases}$$

(b) In order to make $v_f \to v_{fa}$, since there is no control rate to directly control v_f, we design the virtual bow swing angular velocity r_{fa} such that

$$\lim_{t\to\infty} \left\| v_f - v_{f\alpha} \right\| = 0$$

(c) In order to make $u_f \to u_{fa}$, $r_f \to r_{fa}$,We change the forward thrust and the yaw angle torque so that

$$\begin{cases} \lim\limits_{t\to\infty} \left\| u_f - u_{f\alpha} \right\| = 0 \\ \lim\limits_{t\to\infty} \left\| r_f - r_{f\alpha} \right\| = 0 \end{cases}$$

III. FORMATION CONTROLLER DESIGN

A. VIRTUAL QUANTITY DESIGN

Based on back-stepping control method, define z_1 and z_2 as:

$$\begin{cases} z_1 = e_x \cos e_\varphi - e_y \sin e_\varphi \\ z_2 = e_x \sin e_\varphi + e_y \cos e_\varphi \end{cases} \tag{6}$$

take the derivative of both sides and we get the following:

$$\begin{cases} \dot{z}_1 = u_{if} + f_1 \cos e_\varphi - f_2 \sin e_\varphi + z_2 r_{if} \\ \dot{z}_2 = v_{if} + f_1 \sin e_\varphi + f_2 \cos e_\varphi - z_1 r_{if} \end{cases} \tag{7}$$

Suppose u_f, v_f are (z_1, z_2) system inputs, $u_{f\alpha}$ and $v_{f\alpha}$ are non-dummy quantities of u_f and v_f, respectively, and define the Lyapunov function $V_1 = \frac{1}{2}{z_1}^2 + \frac{1}{2}{z_2}^2$, the derivative of both sides gives

$$\begin{aligned} \dot{V}_1 = {} & z_1(u_f + f_1 \cos e_\varphi - f_2 \sin e_\varphi + z_2 r_f) \\ & + z_2(v_f + f_1 \sin e_\varphi + f_2 \cos e_\varphi - z_1 r_f) \end{aligned} \tag{8}$$

the expected value of virtual velocity u_{if} and v_{if} are designed as $u_{f\alpha}$ and $v_{f\alpha}$ relatively.

$$\begin{cases} u_{f\alpha} = -k_1 z_1 - f_1 \cos e_\varphi + f_2 \sin e_\varphi \\ v_{f\alpha} = -k_2 z_2 - f_1 \sin e_\varphi - f_2 \cos e_\varphi \end{cases} \tag{9}$$

The velocity error is $e_v = v_{if} - v_{f_\alpha}$. Take the derivative of both sides and we get

$$\begin{aligned} \dot{e}_v = {} & \frac{m_{11}}{m_{22}} u_{if} r_{f_\alpha} - \frac{d_{22}}{m_{22}} v_{if} + k_2(v_{if} + f_1 \sin e_\varphi \\ & + f_2 \cos e_\varphi - z_1 r_{if}) + f_1 \cos e_\varphi (r_{il} - r_{f_\alpha}) \\ & - f_2 \sin e_\varphi (r_{il} - r_{f_\alpha}) \end{aligned} \tag{10}$$

In order to obtain the control goal $\lim\limits_{t\to\infty} e_v = 0$, we choose the Lyapunov function by virtual expectation of the angular velocity of the heading

$$V_{ev} = \frac{1}{2} e_v^2 \tag{11}$$

$$\begin{aligned} & \frac{d_{22}}{m_{22}} v_{if} - k_2 \left(v_{if} + f_1 \sin e_\varphi + f_2 \cos e_\varphi \right) \\ r_{f_\alpha} = {} & \frac{-f_1 \cos e_\varphi r_{il} - k_3 e_v}{\frac{m_{11}}{m_{22}} u_{if} - k_2 z_1 - f_1 \cos e_u + f_2 \sin e_u} \end{aligned} \tag{12}$$

Substitute (12) into the derivative of (11) we can get $\dot{V}_{ev} = -k_3 {e_v}^2 \leqslant 0$, which indicates that e_v is asymptotic stability

Remark 1: The parameters k_1, k_2 and k_3 in equation (9) and (12) affect the convergence rate of velocity error of the unmanned surface vehicle. The larger k_1, k_2 and k_3 lead to the faster convergence rate but at the cost of introducing more measurement noises.

B. POSITION CONTROLLER DESIGN

In the above section, the distance error was designed using the inverse step method for coordinate transformation, and the virtual desired speed was designed based on the distance error. The purpose of this section is to use the design controller to make the actual velocity converge to the virtual

desired velocity. When the velocity error tends to zero, the USVs formation is in a stable state. The velocity error is designed as $e_u = u_{if} - u_{ifa}$. After deriving both sides of the equation, the velocity error equation can be transformed into:

$$\dot{e}_u = \kappa_1 \tau_{iuf} + \phi_1 + \phi_2 \tag{13}$$

where $\kappa_1 = \frac{1}{m_{11}}$, $a = \tau_{iuf}$, $\phi_1 = \frac{m_{22}}{m_{11}} v_{if} r_{if} - \frac{d_{11}}{m_{11}} u_{if} - \dot{u}_{f_\alpha}$, $\phi_2 = \Delta d_u$, which satisfies $\bar{\phi}_2 \leqslant \bar{\delta}$.

Consider the influence of input saturation of underactuated unmanned surface vehicle, the above formula can be transformed into the following formula:

$$\dot{e}_u = \kappa_1 a + \phi_1 + \phi_2 \tag{14}$$

among them, a is the nonlinear saturation characteristic function, $a = g_1 + \tau_{iuf}$. g_1 is expressed as follows:

$$g_1 = \begin{cases} sign(\tau_{iuf})\tau_{iu\max} - \tau_{iuf}, & \left|\tau_{iuf}\right| > \tau_{iu\max} \\ 0, & \left|\tau_{iuf}\right| < \tau_{iu\max} \end{cases} \tag{15}$$

where $\tau_{iu\max}$ is the maximum allowable force value of the actuator. Saturation control and high-twisting control are used in a single USV. According to the above formula, the speed controller is designed as follows:

$$\begin{aligned} \tau_{iuf} &= -\phi_1 - \frac{1}{\kappa_1}(k_{u1}\xi_1(e_u) + \Theta_u) \\ \dot{\Theta}_u &= -k_{u2}\xi_2(e_u) \end{aligned} \tag{16}$$

For more precise control, we have designed $\xi_1(e_u)$ as the sliding surface of the controller and $\xi_2(e_u) = \frac{d\xi_1(e_u)}{de_u}\xi_1(e_u)$ as the partial derivative of $\xi_1(e_u)$ with respect to e_u.

$$\begin{aligned} \xi_1(e_u) &= \frac{e_u}{\|e_u\|^{1/2}} + k_{u3}e_u, k_{u3} > 0 \\ \xi_2(e_u) &= \frac{d\xi_1(e_u)}{de_u}\xi_1(e_u) \\ &= \frac{1}{2}\frac{e_u}{\|e_u\|} + \frac{2}{3}k_{u3}\frac{e_u}{\|e_u\|^{1/2}} + {k_{u3}}^2 e_u \end{aligned} \tag{17}$$

in which k_{u1}, k_{u2} are the adaptive gain greater than 0.

$$\dot{k}_{u1} = \begin{cases} \mu, & k_{u1} \leqslant \mu \\ \bar{k}_{u1} \cdot \|e_u\| \cdot sign(\|e_u\| - \varepsilon_1), & k_{u1} > \mu \end{cases} \tag{18}$$

$$k_{u2} = \eta_u k_{u1} \tag{19}$$

Substitute (16) into (13), we can get

$$\begin{aligned} \dot{e}_u &= -k_{u1}\xi_1(e_u) + \Theta_u \\ \dot{\Theta}_u &= -k_{u2}\xi_2(e_u) + \Delta\dot{d}_u \end{aligned} \tag{20}$$

Theorem 1: In the velocity subsystem, the error e_u can converge to 0 in finite time under the control law (16) and adaptive gain (18) and (19) when appropriate parameter $\mu, k_{u3}, \eta_u, \varepsilon_1, e_u$ are selected.

Proof In this part, we will analyze the stability of the USV system. Select the Lyapunov candidate function as

$$V_1 = \underbrace{\varsigma^T P \varsigma}_{V_{10}} + \underbrace{\frac{1}{2\gamma_1}\left(k_{u1} - k_{u1}^*\right)^2 + \frac{1}{2\gamma_2}\left(k_{u2} - k_{u2}^*\right)^2}_{V_{1ad}} \tag{21}$$

where, k_{u1} and k_{u1}^* are constants greater than 0; $\varsigma = \begin{bmatrix} \xi_1 & \Theta_u \end{bmatrix}^T$, $P = \begin{bmatrix} \lambda^2 + 4\varepsilon_1 & -\lambda \\ -\lambda & 1 \end{bmatrix}$ is a symmetric positive definite matrix, where $\lambda > 0$, $\varepsilon_1 > 0$.

Take the derivative of both sides of (22) to get

$$\begin{aligned} \dot{V}_1 = {} & \dot{\varsigma}^T P \varsigma + \varsigma^T P \dot{\varsigma} + \frac{1}{\gamma_1}\left(k_{u1} - k_{u1}^*\right)\dot{k}_{u1} \\ & + \frac{1}{\gamma_2}\left(k_{u2} - k_{u2}^*\right)\dot{k}_{u2} \end{aligned} \tag{22}$$

make $K_u = k_{u2} - \frac{\Delta\dot{d}_u}{\xi_2}$, $V_{10} = \varsigma^T P \varsigma$ can be turned into:

$$\dot{V}_{10} = -2\dot{\xi}_1 \varsigma^T Q \varsigma \tag{23}$$

in this formula, Q is a symmetric matrix, and $Q = \begin{bmatrix} q_1 & q_2 \\ q_2 & q_3 \end{bmatrix}$;

$$\begin{aligned} q_1 &= k_{u1}\lambda^2 + 4k_{u1}\varepsilon_1 - \lambda K_u = a_1 k_{u1} - \lambda K_u \\ q_2 &= \frac{1}{2}\left(-\lambda^2 - 4\varepsilon_1 - \lambda k_{u1} + K_u\right) = \frac{1}{2}\left(-a_1 - \lambda k_{u1} + K_u\right) \\ q_3 &= \lambda \end{aligned}$$

If $\dot{V}_{10}$ is negative definite, then the matrix Q is positive definite and its determinant has to be greater than zero. If $\det(Q) > 0$ is to be guaranteed, then the root discriminant $\lambda K_u(k_{u1} - \lambda) > 0$. And because $|\Delta d_u| \leqslant \bar{\delta}$, $\left\|\frac{1}{\xi_2}\right\| \leqslant 2$, so $K_u > 0$, then $k_{u2} > 2\bar{\delta}$, $k_{u1} > \lambda$, where the range of K_u is $K_u \in \left[\underline{k_2}, \bar{k_2}\right] = \left[k_{u2} - 2\bar{\delta}, k_{u2} + 2\bar{\delta}\right]$.

Let $k_{u1} = \lambda + \tau$, then the solution of $\det[Q] = 0$ is

$$\begin{aligned} \rho_1^+ &= \lambda k_{u1} + K_u + 2\sqrt{\lambda K_u(k_{u1} - \lambda)} \\ \rho_1^- &= \lambda k_{u1} + K_u - 2\sqrt{\lambda K_u(k_{u1} - \lambda)} \end{aligned} \tag{24}$$

If ρ_1 takes values in the range $\left(p_{1\max}^-, p_{1\min}^+\right)$, then $\det[Q] > 0$. The existence of a root is guaranteed when $\rho_{1\max}^- < P_{1\max}^-$. Let $\underline{k_2} = \kappa^2$, which gives $\bar{\delta}_2 < \lambda\tau\kappa^2$, from which we can deduce $\underline{k_2} > \frac{\bar{\delta}^2}{\lambda\tau}$, hence $k_2 > \frac{\bar{\delta}^2}{\lambda\tau} + 2\bar{\delta}$.

(23) can be turned into

$$\dot{V}_{10} = -2\dot{\xi}_1\|\varsigma\|^2\lambda_{\min}\{Q\} \leqslant -\gamma_1 V_{10}^{1/2} - \gamma_2 V_{10} \tag{25}$$

where $\gamma_1 = \frac{\lambda_{\min}\{Q\}\lambda\lambda_{\min}^{1/2}\{P\}}{\lambda_{\max}\{P\}}$, $\gamma_2 = 2k_{u3}\frac{\lambda_{\min}\{Q\}\lambda}{\lambda_{\max}\{P\}}$, so

$$\dot{V}_{10} \leqslant -\gamma_1 V_{10}^{1/2} \tag{26}$$

Substituting the adaptive gain (18) (19) into (22) can be translated as

$$\begin{aligned} \dot{V}_1 \leqslant {} & -\beta_\eta V_1^{1/2} \\ & + \underbrace{\left(-\frac{1}{\gamma_1}\bar{k}_{u1}\left|e_u\right| sign\left(\left|e_u\right| - \varepsilon_1\right) + \beta_1\right)\left|k_{u1} - k_{u1}^*\right|}_{\zeta_1} \\ & + \underbrace{\left(-\frac{1}{\gamma_2}\eta\bar{k}_{u1}\left|e_u\right| sign\left(\left|e_u\right| - \varepsilon_1\right) + \beta_2\right)\left|k_{u2} - k_{u2}^*\right|}_{\zeta_2} \end{aligned} \tag{27}$$

where $\beta_\eta = \min\{\eta_1, \beta_1, \beta_2\}$, $\beta_1 = \frac{1}{\gamma_1}k_{u1}^*$, $\beta_2 = \frac{1}{\gamma_2}k_{u2}^*$

In order for k_{u1} and k_{u2} to grow at the slopes of $\bar{k}_{u1}|e_u|$ and $\eta_u\bar{k}_{u1}|e_u|$ respectively, $|e_u| > \varepsilon_1$ has to be satisfied, when the following conditions are met:

$$\gamma_1 < \frac{\bar{k}_{u1}\varepsilon_1}{\beta_1}, \gamma_2 < \frac{\eta_u\bar{k}_{u1}\varepsilon_1}{\beta_2} \tag{28}$$

We can get $\zeta_1 > 0$ and $\zeta_2 > 0$, so $\dot{V}_1 \leqslant -\beta_\eta V_1^{1/2} + \zeta_1 + \zeta_2 \leqslant -\beta_\eta V_1^{1/2}$, $|e_u|$ can converge to $|e_u| > \varepsilon_1$ in finite time, if $|e_u| < \varepsilon_1$, then $\zeta_1 < 0$ and $\zeta_2 < 0$, the state of $\dot{V}_1$ is unknown. The rate of change in gain is going to be $-\bar{k}_{u1}|e_u|$ and $-\eta_u\bar{k}_{u1}|e_u|$. So when the gain goes down to interval $|e_u| > \varepsilon_1$, the gains will increase at the slope of $\bar{k}_{u1}|e_u|$ and $\eta_u\bar{k}_{u1}|e_u|$.

Remark 2: When the velocity error is greater than ε_1, the adaptive gain $\dot{k}_{u1}$ remains unchanged at a fixed value. When the velocity error e_u is less than ε_1, the adaptive gain $\dot{k}_{u1}$ decreases with a small slope. To speed up the convergence rate, ε_1 should be given a small value. The parameter $\bar{k}_{u1}$ determines how fast the adaptive gain decreases, which should depend on the control effect. In order to avoid singularities in the system, the parameter μ is as small as possible in the range of values. The parameter k_{u3} in the equation relate to the rate of growth of the adaptive gain. A larger k_{u3} results in faster growth of the adaptive gain and a more dramatic response to changes in error, but at the cost of introducing more measurement noise. The parameter η_u is the ratio between the respective adaptive gains k_{u1} and k_{u2}, which should depend on the control effect.

C. ATTITUDE CONTROLLER DESIGN

Define the angular velocity error $e_r = r_{if} - r_{f_\alpha}$, take the derivative of both sides:

$$\dot{e}_r = \frac{m_{11} - m_{22}}{m_{33}}u_{if}v_{if} - \frac{d_{33}}{m_{33}}r_{if} + \frac{1}{m_{33}}\tau_{irf} - \dot{r}_{f_\alpha} \tag{29}$$

Consider the effects of unknown external disturbances Δd_r, we get the velocity error equation:

$$\dot{e}_r = \kappa_2\tau_{irf} + \phi_3 + \phi_4 \tag{30}$$

where $\kappa_2 = \frac{1}{m_{33}}$, $\phi_3 = \frac{m_{11}-m_{22}}{m_{33}}u_{if}v_{if} - \frac{d_{33}}{m_{33}}r_{if} - \dot{r}_d$, $\phi_4 = \Delta d_r$ is the external interference of the angular velocity ring, and meet $\bar{\phi}_3 \leqslant \bar{\delta}$.

Among them b is nonlinear saturation characteristic function. $b = g_2 + \tau_{irf}$, g_2 is expressed as follows:

$$g_2 = \begin{cases} sign(\tau_{irf})\tau_{ir\max} - \tau_{irf}, & |\tau_{irf}| > \tau_{ir\max} \\ 0, & |\tau_{irf}| < \tau_{ir\max} \end{cases} \tag{31}$$

$\tau_{ir\max}$ is the maximum allowable torque value of the actuator.

According to the formula, the angular velocity controller is designed as follows:

$$\tau_{irf} = -\phi_3 - \frac{1}{\kappa_2}(k_{r1}\xi_1(e_r) + \Theta_r)$$

$$\dot{\Theta}_r = k_{r2}\xi_2(e_r) \tag{32}$$

For more precise control, we have designed $\xi_1(e_r)$ as the sliding surface of the controller and $\xi_2(e_r) = \frac{d\xi_1(e_r)}{de_r}\xi_1(e_r)$ as the partial derivative of $\xi_1(e_r)$ with respect to e_r.

$$\begin{aligned} \xi_1(e_r) &= \frac{e_r}{\|e_r\|^{1/2}} + k_{r3}e_r, k_{r3} > 0 \\ \xi_2(e_r) &= \frac{d\xi_1(e_r)}{de_r}\xi_1(e_r) \\ &= \frac{1}{2}\frac{e_r}{\|e_r\|} + \frac{2}{3}k_{r3}\frac{e_r}{\|e_r\|^{1/2}} + {k_{r3}}^2 e_r \end{aligned} \tag{33}$$

k_{r1}, k_{r2} is the adaptive gain greater than 0.

$$\dot{k}_{r1} = \begin{cases} \sigma, & k_{r1} \leqslant \sigma \\ \bar{k}_{r1} \cdot \|e_r\| \cdot sign(\|e_r\| - \varepsilon_2), & k_{r1} > \sigma \end{cases} \tag{34}$$

$$k_{r2} = \eta_r k_{r1} \tag{35}$$

Substitude (33) into formula (31)

$$\begin{aligned} \dot{e}_r &= -k_{r1}\xi_1(e_r) + \Theta_r \\ \dot{\Theta}_r &= -k_{r2}\xi_2(e_r) + \Delta\dot{d}_r \end{aligned} \tag{36}$$

Theorem 2: In the attitude subsystem, the attitude angle tracking error e_r can converge to 0 in finite time under the attitude controller (32) and adaptive gain (34) and (35) when appropriate parameter $\sigma, k_{r3}, \eta_r, \varepsilon_3, e_r, \bar{k}_{r1}$.

Proof In this part, the stability of the USV system will be analyzed, select the Lyapunov candidate function:

$$V_2 = \underbrace{\varsigma^T P_2 \varsigma}_{V_{20}} + \underbrace{\frac{1}{2\gamma_3}\left(k_{r1} - k_{r1}^*\right)^2 + \frac{1}{2\gamma_4}\left(k_{r2} - k_{r2}^*\right)^2}_{V_{2ad}} \tag{37}$$

k_{r1} and k_{r1}^* are constants greater than 0; $\varsigma_2 = \begin{bmatrix} \xi_2 & \Theta_r \end{bmatrix}^T$, $P_2 = \begin{bmatrix} {\lambda_2}^2 + 4\varepsilon_2 & -\lambda_2 \\ -\lambda_2 & 1 \end{bmatrix}$ is a symmetric positive definite matrix, among them $\lambda_2 > 0, \varepsilon_2 > 0$.

Take the derivative of both sides of (38) to get

$$\begin{aligned} \dot{V}_2 = {} & \dot{\varsigma}_2^T P_2 \varsigma_2 + {\varsigma_2}^T P_2 \dot{\varsigma}_2 + \frac{1}{\gamma_3}\left(k_{r1} - k_{r1}^*\right)\dot{k}_{r1} \\ & + \frac{1}{\gamma_4}\left(k_{r2} - k_{r2}^*\right)\dot{k}_{r2} \end{aligned} \tag{38}$$

Let $K_r = k_{r2} - \frac{\Delta\dot{d}_r}{\xi_2}$, then $V_{20} = \varsigma^T P\varsigma$ can be reduced to

$$\dot{V}_{20} = -2\xi_1'\varsigma^T Q\varsigma \tag{39}$$

where Q is a symmetric matrix and $Q = \begin{bmatrix} q_1 & q_2 \\ q_2 & q_3 \end{bmatrix}$;

$$\begin{aligned} q_1 &= k_{r1}\lambda^2 + 4k_{r1}\varepsilon - \lambda K_r = a_1 k_{r1} - \lambda K_r \\ q_2 &= \frac{1}{2}\left(-\lambda^2 - 4\varepsilon - \lambda k_{r1} + K_r\right) = \frac{1}{2}\left(-a_1 - \lambda k_{r1} + K_r\right) \\ q_3 &= \lambda \end{aligned}$$

If $\dot{V}_{20}$ is negative definite, then the matrix Q is positive definite and its determinant has to be greater than zero. If $\det(Q) > 0$ is to be guaranteed, then the root discriminant

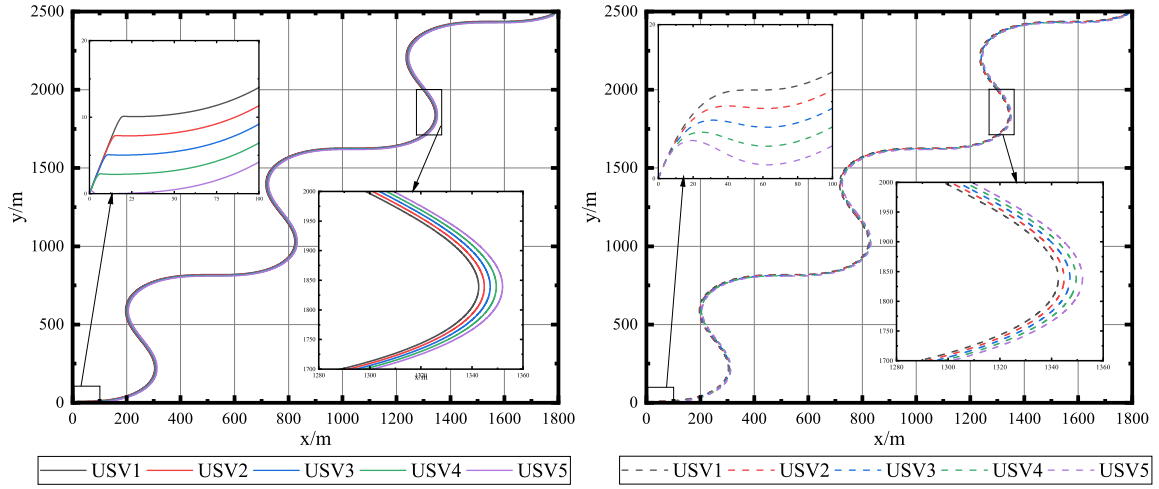

FIGURE 4. Formation trajectory diagram with IS-STW and AB-NDO.

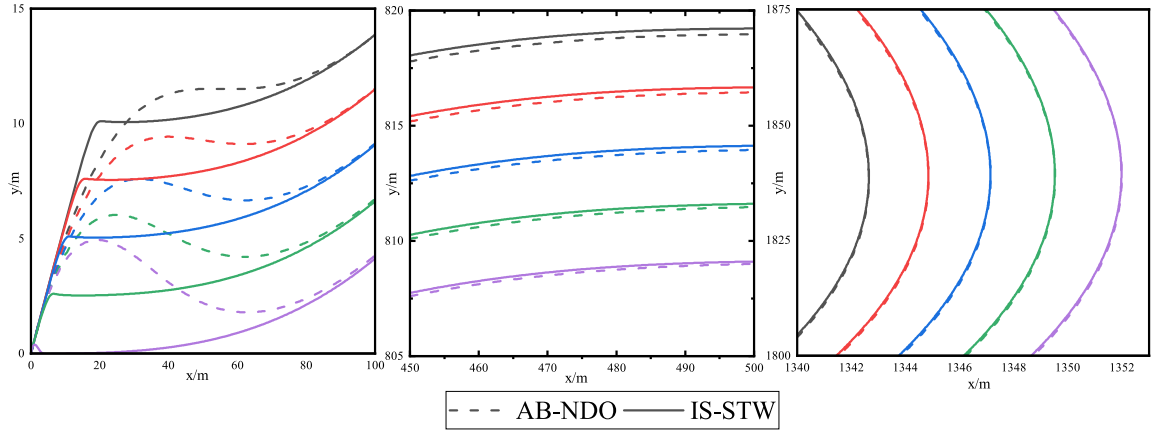

FIGURE 5. Formation detail trajectory diagram.

$\lambda K_r(k_{r1}-\lambda) > 0$. Again, because $|\Delta d_r| \leqslant \bar{\delta}$, $\left\|\frac{1}{\xi_2}\right\| \leqslant 2$, so $K_r > 0$, and thus $k_{r2} > 2\bar{\delta}$, $k_{r1} > \lambda$. where K_r takes values in the range $K_r \in \left[\underline{k_2}, \bar{k}_2\right] = \left[k_{r2}-2\bar{\delta}, k_{r2}+2\bar{\delta}\right]$.

Let $k_{r1} = \lambda + \tau$ where $\tau > 0$. Then the solution for $\det[Q] = 0$ is

$$\begin{aligned}\rho_1^+ &= \lambda k_{r1} + K_r + 2\sqrt{\lambda K_r\,(k_{r1}-\lambda)}\\ \rho_1^- &= \lambda k_{r1} + K_r - 2\sqrt{\lambda K_r\,(k_{r1}-\lambda)}\end{aligned} \tag{40}$$

If ρ_1 takes values in the range $\left(p_{1\max}^-, p_{1\min}^+\right)$, then $\det[Q] > 0$. The existence of a root is guaranteed when $\rho_{1\max}^- < P_{1\max}^-$. Let $\underline{k_2} = \kappa^2$ and we have $\bar{\delta}_2 < \lambda\tau\kappa^2$, from which we deduce that $\underline{k_2} > \frac{\bar{\delta}^2}{\lambda\tau}$, hence $K_r > \frac{\bar{\delta}^2}{\lambda\tau} + 2\bar{\delta}$.

Let the maximal and minimal eigenvalues of the $\lambda_{\max}\{P\}$ and $\lambda_{\min}\{P\}$, on matrix P such that (3) can be reduced to

$$\dot{V}_{20} = -2\xi_1'\|\varsigma\|^2\lambda_{\min}\{Q\} \leqslant -\gamma_1 V_{20}^{1/2} - \gamma_2 V_{20} \tag{41}$$

where $\gamma_3 = \frac{\lambda_{\min}\{Q\}\lambda\lambda_{\min}^{1/2}\{P\}}{\lambda_{\max}\{P\}}$, $\gamma_4 = 2k_{r3}\frac{\lambda_{\min}\{Q\}\lambda}{\lambda_{\max}\{P\}}$.

Therefore, we gain

$$\dot{V}_{20} \leqslant -\gamma_1 V_{20}^{1/2} \tag{42}$$

Substituting the adaptive gain (34)(35) into (38) can be transformed into

$$\begin{aligned}\dot{V}_2 \leqslant\ & -\beta_\eta V_2^{1/2}\\ &+ \underbrace{\left(-\frac{1}{\gamma_3}\bar{k}_{r1}\,|e_r|\,sign\,(|e_r|-\varepsilon_2)+\beta_3\right)\left|k_{r1}-k_{r1}^*\right|}_{\zeta_3}\\ &+ \underbrace{\left(-\frac{1}{\gamma_4}\eta\bar{k}_{r1}\,|e_r|\,sign\,(|e_u|-\varepsilon_2)+\beta_4\right)\left|k_{r2}-k_{r2}^*\right|}_{\zeta_4}\end{aligned} \tag{43}$$

where $\beta_\eta = \min\{\eta_2, \beta_3, \beta_4\}$, $\beta_3 = \frac{1}{\gamma_3}k_{r1}^*$, $\beta_4 = \frac{1}{\gamma_4}k_{r2}^*$

In order for k_{r1} and k_{r2} to grow at the slopes of $\bar{k}_{r1}\,|e_r|$ and $\eta_r\bar{k}_{r1}\,|e_r|$ respectively, $|e_r| > \varepsilon_2$ has to be satisfied. When the

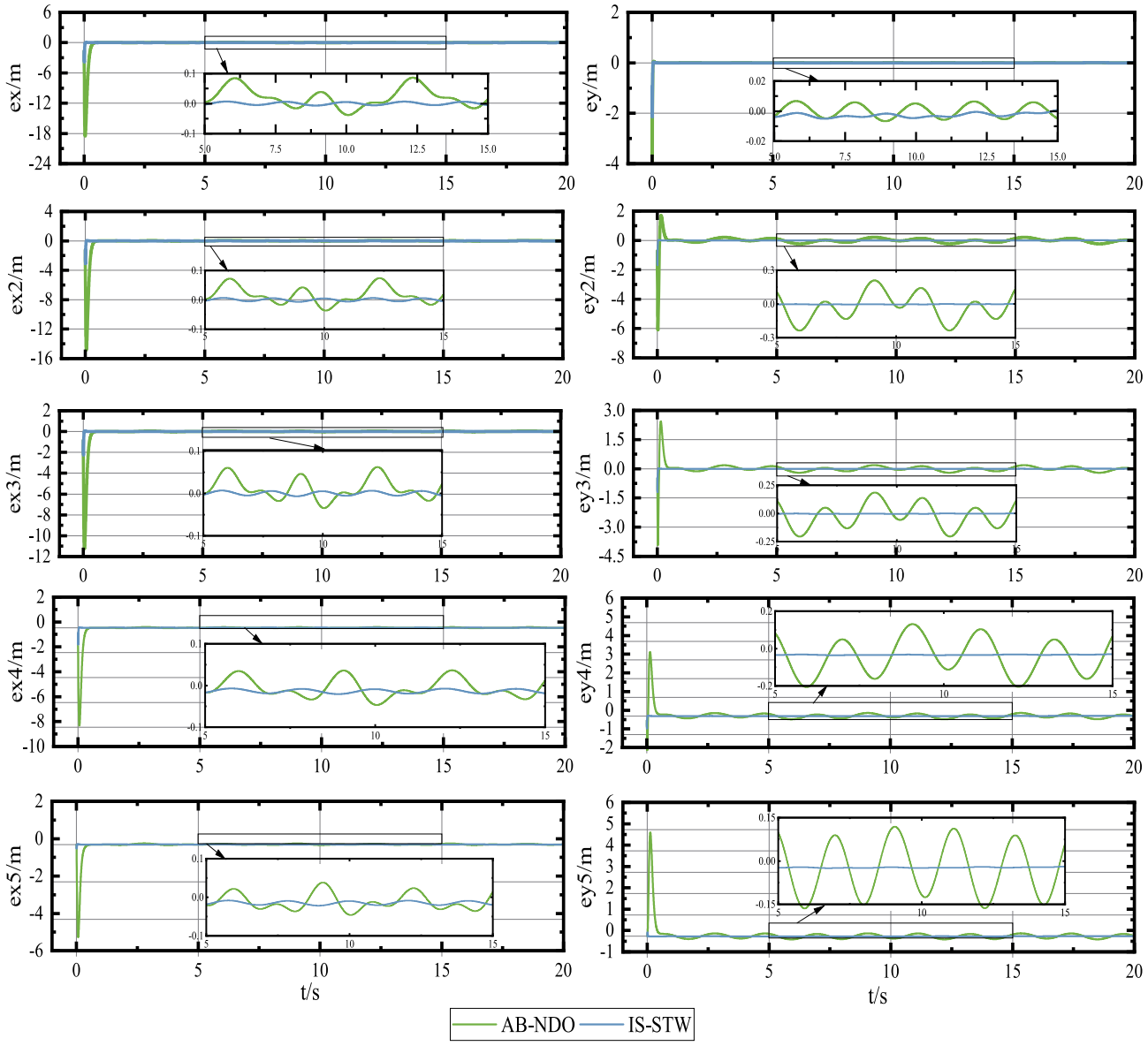

FIGURE 6. Position error diagram of USV ith (i=1,2,3,4,5).

following conditions are met:

$$\gamma_3 < \frac{\bar{k}_{r1}\varepsilon_2}{\beta_3}, \gamma_4 < \frac{\eta_r \bar{k}_{r1}\varepsilon_2}{\beta_4} \tag{44}$$

we can get $\zeta_3 > 0$ and $\zeta_4 > 0$.

Therefore $\dot{V}_2 \leqslant -\beta_\eta V_2^{1/2} + \zeta_3 + \zeta_4 \leqslant -\beta_\eta V_2^{1/2}$, so $|e_r|$ can converge to $|e_r| > \varepsilon_2$ in finite time; if $|e_r| < \varepsilon_2$, then $\zeta_3 < 0$, $\zeta_4 < 0$. The plus or minus of $\dot{V}_2$ is unknown. The rate of change in gain is going to be $-\bar{k}_{r1}|e_r|$ and $-\eta_r \bar{k}_{r1}|e_r|$, so when the gain goes down to interval $|e_r| > \varepsilon_2$, the gains will increase at the slope of $\bar{k}_{r1}|e_r|$ and $\eta_r \bar{k}_{r1}|e_r|$.

Remark 3: When the velocity error is greater than ε_2, the adaptive gain $\dot{k}_{r1}$ remains unchanged at a fixed value. When the velocity error e_r is less than ε_2, the adaptive gain $\dot{k}_{r1}$ decreases with a small slope. To speed up the convergence rate, ε_2 should be given a small value. The parameter $\bar{k}_{r1}$ determines how fast the adaptive gain decreases, which should depend on the control effect. In order to avoid singularities in the system, the parameter σ is as small as possible in the range of values. The parameter k_{r3} in the equation relate to the rate of growth of the adaptive gain. A larger k_{r3} results in faster growth of the adaptive gain and a more dramatic response to changes in error, but at the cost of introducing more measurement noise. The parameter η_r is the ratio between the respective adaptive gains k_{r1} and k_{r2}, which should depend on the control effect.

IV. SIMULATION

A. SIMULATION PARAMETER SETTING

The designed adaptive super-twisting controller is simulated.

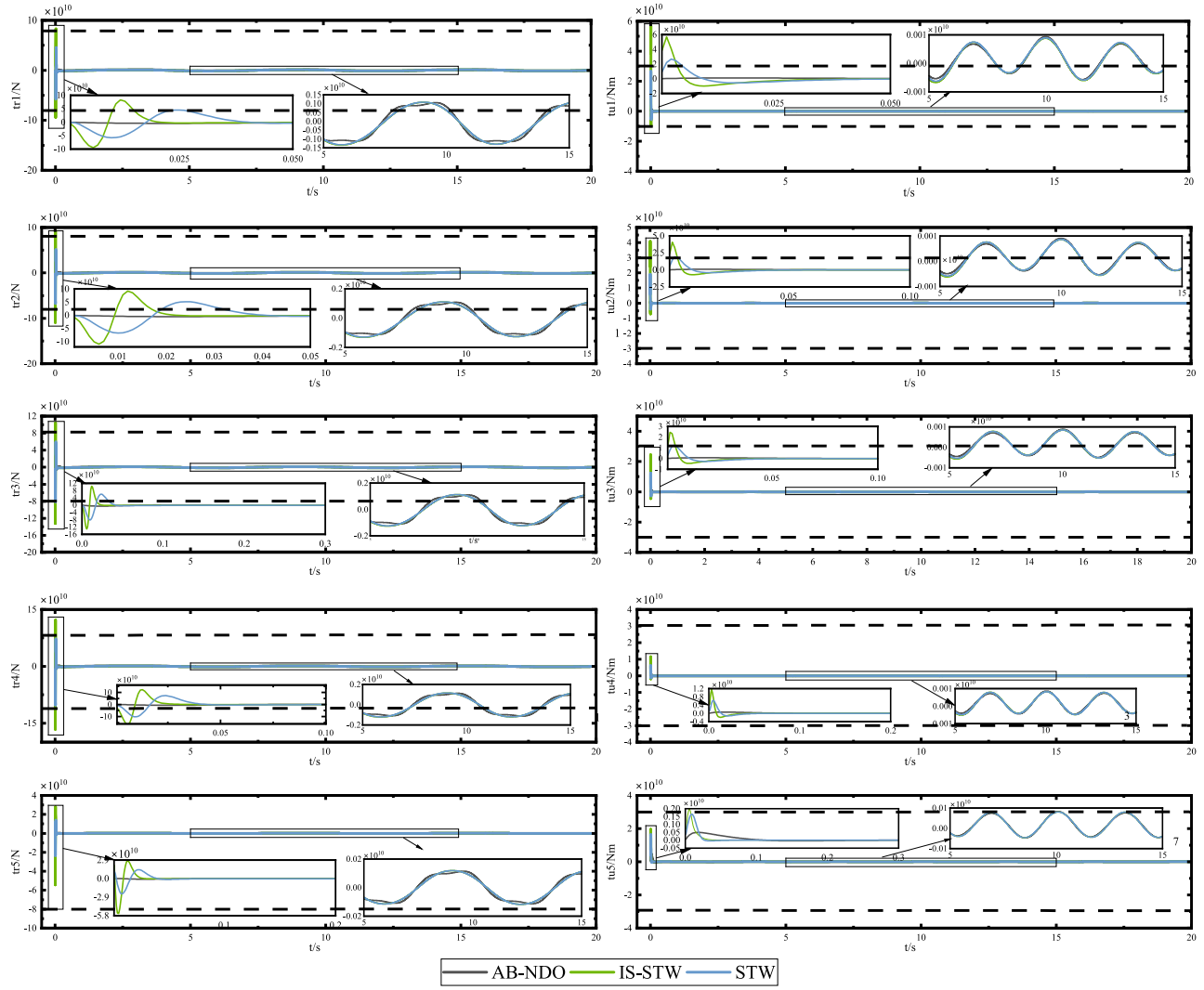

FIGURE 7. Control law diagram of USV ith (i=1,2,3,4,5).

TABLE 1. Control parameter setting.

parameter	parameter	parameter	parameter
k_1	15	ε_1	0.01
k_2	15	ε_2	0.01
k_3	15	η_u	1
k_{u3}	20	η_r	1
k_{v3}	20	μ	0.2
$\bar{k}_{u1}$	5	σ	0.2
$\bar{k}_{v1}$	5	$tu_{\max}$	$\pm 3 \times 10^{10}$
$tr_{\max}$	$\pm 8 \times 10^{10}$		

The USV parameters are:

$$m_{11} = 1.2 \times 10^5 kg, d_{11} = 2.15 \times 10^4 kg$$
$$m_{22} = 2.179 \times 10^5 kg, d_{22} = 1.17 \times 10^3 kg \cdot s^{-1}$$
$$m_{33} = 6.36 \times 10^7 kg, d_{33} = 8.02 \times 10^6 kg \cdot s^{-1}$$

In order to verify the feasibility of the formation keeping algorithm in this paper, time-varying reference trajectory is used to test the performance of formation. Consider the case that the initial position of the virtual leader is $P_{L0} = [x_{L0}, y_{L0}, \varphi_{L0}]^T = [0, 0, 0]^T$. The dynamics of the virtual leader is described by

$$\begin{cases} \dot{x}_L = u_L \cos(\varphi_L) - v_L \sin(\varphi_L) \\ \dot{y}_L = u_L \sin(\varphi_L) + v_L \cos(\varphi_L) \\ \dot{\varphi}_L = r_L \end{cases} \tag{45}$$

The variable $x_L, y_L, \varphi_L, u_L, v_L, r_L$ are the position and the velocity of the virtual leader. Where $u_L = 200$, $v_L = t$, $r_L = 0$, $v_l = \sin(t)$, The initial positions of the USVs are selected as Table.2.Since the external disturbance is related to the environmental changes of the unmanned boat sailing and the external wind and wave current loads, we define the external disturbance as a sinusoidal function $\Delta d_r = 3\sin(3t)$, and $\Delta d_u = 3\sin(3t)$ to test and compare the response speed and immunity of the system to the external disturbance. The parameters are set as shown in the table 2, and the

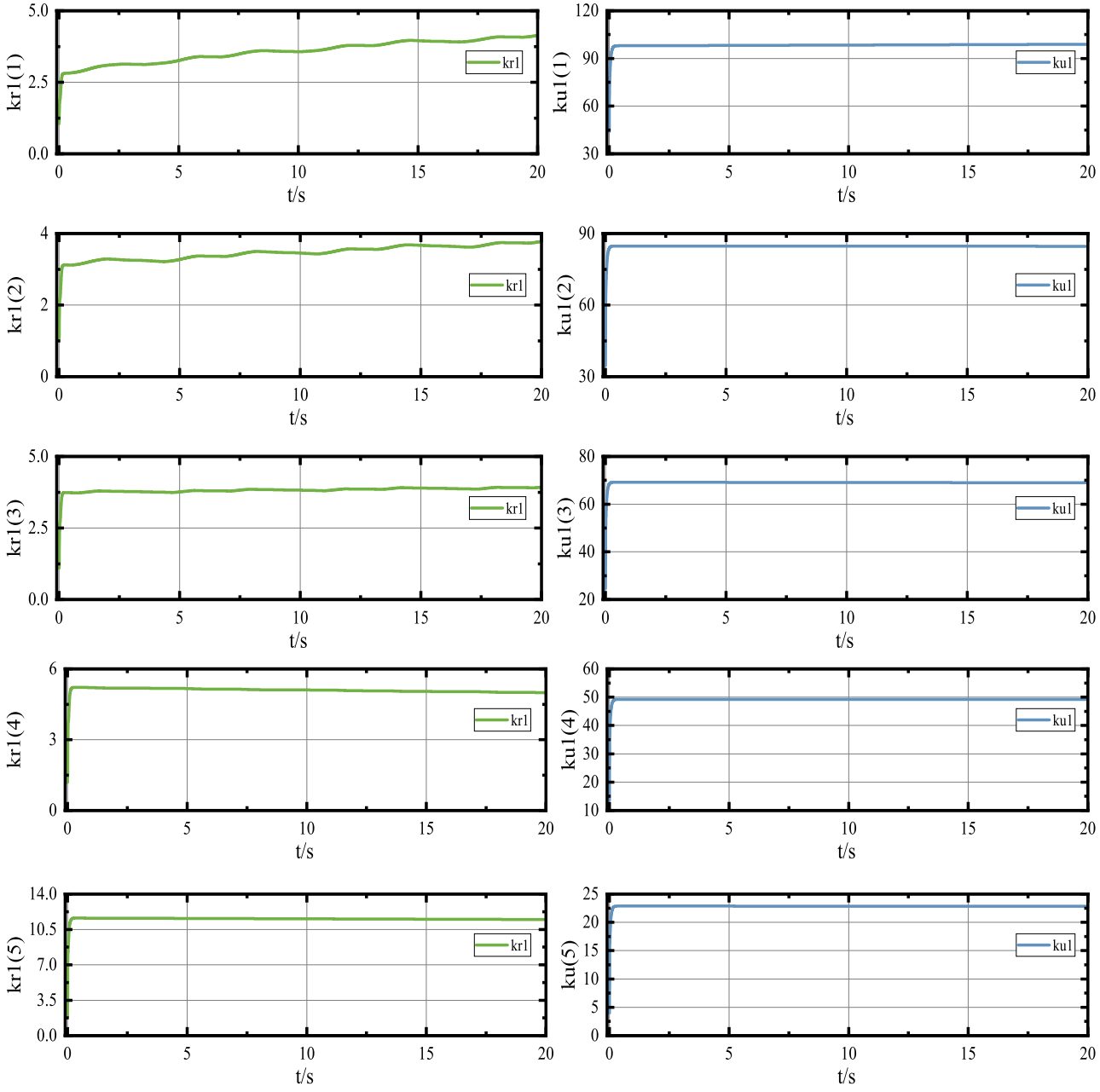

FIGURE 8. Control gain diagram of USV ith (i=1,2,3,4,5).

parameters are selected by referring to **Remark 1**, **Remark 2** and **Remark 3**. The proposed algorithm is compared with an adaptive back-stepping control formation strategy based on a nonlinear disturbance observer in literature [25]. Its control parameters are shown below, $k_{ri} = 20, k_{\varphi i} = 2, k_{ui} = 20, k_{dui} = 15, k_{dri} = 15, \lambda_{u0i} = \lambda_{r0i} = 10$, $\lambda_{u1i} = \lambda_{r1i} = 0.1$.

B. THE SIMULATION RESULTS

Figure 4 - Figure 5 show the trajectory of USV formation based on the leader-follower method of back-stepping formation control of unmanned surface vehicles with input saturation based on adaptive super-twisting algorithm (IS-STW) and adaptive backstepping control formation strategy based on a nonlinear disturbance observer (AB-NDO) in [26]. The solid line is IS-STW and the dash line is AB-NOD. Figure 6 describe the lateral and longitudinal

TABLE 2. Formation settings.

USV number	x	y	Expected distance L_d	Expected Angle θ_d
1	0	0	20	$\pi/6$
2	0	0	15	$\pi/6$
3	0	0	10	$\pi/6$
4	0	0	5	$\pi/6$
5	0	0	0	$\pi/6$

position error of the USVs under IS-STW control and AB-NDO under external disturbances. Figure 7 describe the control efforts of the USVs with time of the USVs under IS-STW method and without input saturation method. Figure 8 describe the control gain of the each USV in the formation.

It can be clearly observed from Figure 4 the two methods all can ensure satisfactory control performance under complex practical applications. The performance of formation strongly verifies the validity of back-stepping formation scheme. Meanwhile, our proposed method can still ensure the best comprehensive control performance compared with the AB-NOD control schemes as indicated in Figure 5. At the beginning, the USVs can form a stable formation more quickly under the IS-STW method, which shows the effectiveness of the proposed control more specifically. When voyaging in straight line and curve line with external disturbance, the formation of the USVs under IS-STW control is kept more perfect, which shows that our method is able to respond more rapidly to external disturbances.

As can be seen in Figure 6, when there are large error between the initial position and the desired position, the trajectory error of the USVs under IS-STW control converges at 0.05s seconds, while the error converges in more than 0.4s under AB-NDO control. When the formation is asymptotically stable, the trajectory error of the USV under IS-STW control is much smaller under external perturbations, indicating that our adaptive gain and controller are better able to deal with time-varying external environments and have higher control accuracy.

In Figure 7, the velocity of convergence is more quickly and the force and moment of is bigger under the IS-STW method, which represents the USV with our proposed method can highly resistant to the external disturbance. Furthermore, the torque under saturation control always remains within the range of the upper and lower bounds $\pm 3 \times 10^{10}$, $\pm 8 \times 10^{10}$, which means that saturation control can successfully limit the input to a safe range. Our approach additionally avoids the problem of input overload while ensuring good control accuracy and fast convergence of errors in the controller.

As can be seen in Figure 8, the derivative of the adaptive gain $\dot{k}_{u1}$ remains constant at a fixed value when the velocity error is greater than ε_1. When the speed error e_u is less than ε_1, the derivative of the adaptive gain $\dot{k}_{u1}$ decreases with the decrease of the error. Since the error varies abruptly because of external disturbances, the adaptive gain changes from moment to moment in order to maintain the stability of the formation. The change rule of the adaptive gain $\dot{k}_{r1}$ is the same as $\dot{k}_{u1}$.

V. CONCLUSION

In this paper, we have solved the problem of the formation of multiple unmanned surface vehicles under input overload and external disturbance. Firstly, the modelling of underactuated USVs formation and the design of virtual desired velocity are completed using the leader-follower and back-stepping methods. Secondly, the proposed adaptive super-twisting algorithm is used to compensate for parameter uncertainties and unknown external disturbances in the dynamics model. In addition, an input saturation function is constructed to prevent the input overload problem during the navigation of USV. Finally, the effectiveness of the proposed control law is verified by simulations. Simulation results show that the controller can roughly keep the trajectory of the USV consistent with the expected trajectory and ensure that the input values are within the safe range. In the formation of multiple unmanned surface vehicles, this controller not only can achieve the USV trajectory while keeping the formation stable, but also can maintain the stable dynamic performance of the USV during navigation and avoid the problems of input overload and jitter, which proves the effectiveness of the method in this paper.

REFERENCES

[1] Y. Zhao, Y. Ma, and S. Hu, "USV formation and path-following control via deep reinforcement learning with random braking," *IEEE Trans. Neural Netw. Learn. Syst.*, vol. 32, no. 12, pp. 5468–5478, Dec. 2021.

[2] W. Zhou, Y. Wang, C. K. Ahn, J. Cheng, and C. Chen, "Adaptive fuzzy backstepping-based formation control of unmanned surface vehicles with unknown model nonlinearity and actuator saturation," *IEEE Trans. Veh. Technol.*, vol. 69, no. 12, pp. 14749–14764, Dec. 2020.

[3] X. Sun, G. Wang, Y. Fan, D. Mu, and B. Qiu, "A formation collision avoidance system for unmanned surface vehicles with leader-follower structure," *IEEE Access*, vol. 7, pp. 24691–24702, 2019.

[4] Z. L. Ouyang, H. Wang, Y. Huang, K. Yang, and H. Yi, "Path planning technologies for USV formation based on improved RRT," *Chin. J. Ship Res.*, vol. 15, no. 3, pp. 18–24, 2020.

[5] D. Wang and M. Fu, "Adaptive formation control for waterjet USV with input and output constraints based on bioinspired neurodynamics," *IEEE Access*, vol. 7, pp. 165852–165861, 2019.

[6] F. Deng, L. Jin, X. Hou, L. Wang, B. Li, and H. Yang, "COLREGs: Compliant dynamic obstacle avoidance of USVs based on the dynamic navigation ship domain," *J. Mar. Sci. Eng.*, vol. 9, no. 8, p. 837, Aug. 2021.

[7] X. Liang, C. Xu, and D. Wang, "Adaptive neural network control for marine surface vehicles platoon with input saturation and output constraints," *AIMS Math.*, vol. 5, no. 1, pp. 587–602, 2020, doi: 10.3934/MATH.2020039.

[8] X. Liang and N. Wang, "Adaptive leader–follower formation for unmanned surface vehicles subject to output constraints," *Int. J. Fuzzy Syst.*, vol. 22, no. 8, pp. 2493–2503, Nov. 2020.

[9] M.-Y. Fu, D.-S. Wang, and C.-L. Wang, "Formation control for water-jet USV based on bio-inspired method," *China Ocean Eng.*, vol. 32, no. 1, pp. 117–122, Mar. 2018.

[10] X. Yan, D. Jiang, R. Miao, and Y. Li, "Formation control and obstacle avoidance algorithm of a multi-USV system based on virtual structure and artificial potential field," *J. Mar. Sci. Eng.*, vol. 9, no. 2, p. 161, Feb. 2021.

[11] Z. Sun, G. Zhang, and L. Qiao, "Robust adaptive trajectory tracking control of underactuated surface vessel in fields of marine practice," *J. Mar. Sci. Technol.*, vol. 23, no. 4, pp. 950–957, 2018.

[12] Z. Piao, C. Guo, and S. Sun, "Adaptive backstepping sliding mode dynamic positioning system for pod driven unmanned surface vessel based on cerebellar model articulation controller," *IEEE Access*, vol. 8, pp. 48314–48324, 2020.

[13] Y. Zhao, X. Sun, and G. Wang, "Adaptive back-stepping sliding mode tracking control for underactuated unmanned surface vehicle with disturbances and input saturation," *IEEE Access*, vol. 9, pp. 1304–1312, 2020.

[14] H. Jianzhang, T. Guoyuan, W. Jianjun, and X. De, "Swarm control of USVs based on adaptive back-stepping combined with sliding mode," *Chin. J. Ship Res.*, vol. 14, no. 6, pp. 1–7, 2019, doi: 10.19693/J.ISSN.1673-3185.01521.

[15] R. Rout and B. Subudhi, "A back-stepping approach for the formation control of multiple autonomous underwater vehicles using a leader-follower strategy," *J. Mar. Eng. Technol.*, vol. 15, no. 1, pp. 38–46, 2016.

[16] Y. El Houm, A. Abbou, M. Labbadi, and M. Cherkaoui, "Optimal new sliding mode controller combined with modified supertwisting algorithm for a perturbed quadrotor UAV," *Int. J. Aerosp. Eng.*, vol. 2020, pp. 1–10, Nov. 2020.
[17] B. Brogliato, A. Polyakov, and D. Efimov, "The implicit discretization of the supertwisting sliding-mode control algorithm," *IEEE Trans. Autom. Control*, vol. 65, no. 8, pp. 3707–3713, Aug. 2019.
[18] M. V. Basin and P. C. R. Ramírez, "A supertwisting algorithm for systems of dimension more than one," *IEEE Trans. Ind. Electron.*, vol. 61, no. 11, pp. 6472–6480, Jan. 2014.
[19] B. Tian, J. Cui, H. Lu, L. Liu, and Q. Zong, "Attitude control of UAVs based on event-triggered supertwisting algorithm," *IEEE Trans. Ind. Informat.*, vol. 17, no. 2, pp. 1029–1038, Feb. 2021.
[20] M. Jouini, S. Dhahri, and A. Sellami, "Design of robust supertwisting algorithm based second-order sliding mode controller for nonlinear systems with both matched and unmatched uncertainty," *Complexity*, vol. 2017, pp. 1–8, Dec. 2017.
[21] P. Singh, A. Nandanwar, L. Behera, N. K. Verma, and S. Nahavandi, "Uncertainty compensator and fault estimator-based exponential supertwisting sliding-mode controller for a mobile robot," *IEEE Trans. Cybern.*, vol. 52, no. 11, pp. 1–14, Nov. 2021.
[22] B. Qiu, G. Wang, Y. Fan, D. Mu, and X. Sun, "Path following of underactuated unmanned surface vehicle based on trajectory linearization control with input saturation and external disturbances," *Int. J. Control Automat. Syst.*, vol. 18, pp. 2108–2119, Feb. 2020.
[23] D. D. Mu, G. F. Wang, Y. S. Fan, B. B. Qiu, and X. J. Sun, "Adaptive course control based on trajectory linearization control for unmanned surface vehicle with unmodeled dynamics and input saturation," *Neurocomputing*, vol. 330, pp. 1–10, Feb. 2019.
[24] H. Deng, R. Wang, J. Li, and D. Chen, "RBF neural network control for USV with input saturation," in *Proc. MATEC Web Conf.*, vol. 214, 2018, Art. no. 03002.
[25] C. Zhang and Q. Dong, "Adaptive gain sliding mode control for fixed-wing UAV with input saturation," *Acta Aeronautica et Astronautica Sinica*, vol. 41, no. S1, pp. 79–87, 2020.
[26] Y. Fan, X. Shen, D. Mu, G. Wang, and Y. Zhao, "Formation control of unmanned surface vehicle for actuator failure," in *Proc. 34th Chin. Control Decis. Conf.*, 2022, pp. 457–462, doi: 10.26914/c.cnkihy.2022.020833.

ZOU YUHAN is currently pursuing the Bachelor of Engineering degree with the Hubei University of Technology (HBUT), Wuhan. She is also pursuing her research under Dr. Wei Shang. She helped complete a few projects in the fields of formation control, stability analysis, and super-twisting.

WANG KUN received the master's degree from Beihang University, Beijing, China, in 2016. He is currently an Engineer with the China Ship Development and Design Center. His research interests include unmanned system design and reliability systems engineering.

SHANG WEI received the Ph.D. degree in aeronautical and astronautical science and technology from the Beijing Institute of Technology, China, in 2017. He is currently a Lecturer with the Hubei University of Technology. His research interests include control theory of multi-agent systems and fight control.

LIU ZHOU is currently pursuing the Bachelor of Engineering degree with the Hubei University of Technology (HBUT), Wuhan. He is also pursuing his research under Dr. Wei Shang. He helped complete lots of jobs of spacecrafts, which include distributed control, attitude control, and trajectory tracking.

ZHENG ZHONGZHONG is currently pursuing the Bachelor of Engineering degree with the Hubei University of Technology (HBUT), Wuhan. He is also pursuing his research under Dr. Wei Shang. He helped complete lots of jobs of quadrotor, which include distributed control, nested adaptive, and trajectory tracking.

JING GUO HAO is currently pursuing the degree with the Hubei University of Technology (HBUT), Wuhan. He is also pursuing his research under Dr. Wei Shang and he has completed a few projects in the fields of quadrotors control, stability analysis, and data processing. His research interests include distributed control, nested adaptive, and formation control.